Airborne Thermal Infrared Hyperspectral Imaging for Mineral Mapping

Minerals such as silicates, aluminosilicates (feldspar), magnesium silicates (serpentine) and olivines are among the most commonly encountered in the environment. Airborne mineral mapping of these minerals using conventional visible-near infrared (VNIR, 0.4-1.4 µm) and shortwave infrared (SWIR, 1.4-3 µm) sensors can be very challenging since the Si-O bounds are featureless or exhibit very weak spectral features in these spectral ranges. The fundamental vibrations associated with most functional groups composing the different ores mostly occurs in the thermal infrared (TIR, 8-12 µm) spectral range. In order to illustrate the benefits of thermal infrared hyperspectral imaging (HSI) for mineral mapping, an airborne survey was carried out over an open-pit mine in the Thetford Mines (Qc, Canada) area. The results show how the high spectral resolution data provided by the Telops Hyper-Cam airborne system facilitates temperature emissivity separation (TES) and atmospheric correction in order to retrieve a thermodynamic temperature map of the area and its associated spectral emissivity datacube. Mineral mapping of various minerals such as lizardite, serpentinite and quartz was achieved through linear unmixing of the emissivity data using reference emissivity curves found in spectral libraries. The results illustrate the potential of TIR HSI for airborne mapping of silicate minerals.

Introduction

The use of airborne remote sensing techniques to characterize mining environments offers many benefits as it allows coverage of large areas in a very efficient way. Both visible-near infrared (VNIR, 0.4-1.4 µm) and shortwave infrared (SWIR, 1.4-3.0 µm) are well established techniques in this field. In general, the reflectance spectral features measured in the VNIR and SWIR spectral ranges are overtones and/or combination bands from fundamental absorption bands of the longwave infrared (LWIR, 8-12 µm). For this reason, the reflectance features measured by VNIR and SWIR sensors are typically broad and/or suffer from strong overlapping which raises selectivity issues for mineral identification in some cases. Since the spectral features associated with fundamental vibrations are stronger and sharper than their overtones, LWIR may also improve selectivity in certain situations. In addition, the overtone signals of many minerals such as silicate (Si-O), feldspar (Al-O-Si) and olivine ($(Mg,Fe)_2[SiO_4]$) are too weak to give appreciable spectral features in the VNIR and SWIR. As illustrated in Figure 1, these minerals are likely to be encountered in many environments and regions of the world as they result from the geological processes involving the first most abundant elements encountered on Earth. Most silicates, aluminosilicates and magnesium silicate minerals such as quartz (SiO_2), feldspar (Na-feldspar, K-feldspar and Ca-feldspar), serpentine (Mg-O-Si, antigorite, chrysotile and lizardite), olivine (e.g. fayalite and forsterite) have strong absorption and emission bands in the LWIR spectral range.

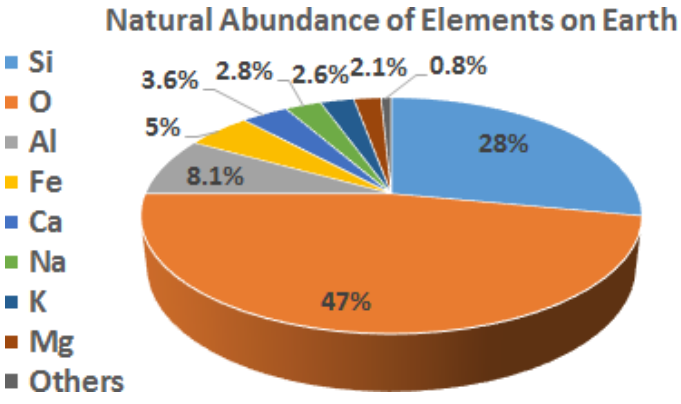

Figure 1 Natural abundance of elements in Earth crust.

In addition, other commonly encountered minerals such as carbonates (e.g. calcite ($CaCO_3$) and dolomite ($CaMg(CO_3)_2$), phosphates (e.g. apatite) and sulfates (e.g. gypsum ($CaSO_4$) and alunite) also have important

spectral features in the LWIR. Therefore, LWIR presents itself as a method of choice for the characterization of minerals.

The inherent self-emission associated with LWIR under ambient conditions allows airborne surveys in various weather (cloudy, partly cloudy or clear sky) and illumination (day or night) conditions. For this reason, LWIR often refers to the thermal infrared (TIR) spectral range. Solid targets such as minerals not only emit but also reflect thermal infrared radiation. Since the two phenomena occur simultaneously, they end-up mixed in the radiance measured at the sensor level as illustrated in Figure 2. The signal also contains spectral features associated with gaseous atmospheric components such as water (H_2O) vapor. For outdoor measurements, target irradiance mostly consists of a combination of sky radiance and the surrounding. The effective irradiance of the target often refers to the downwelling (DW) radiance.

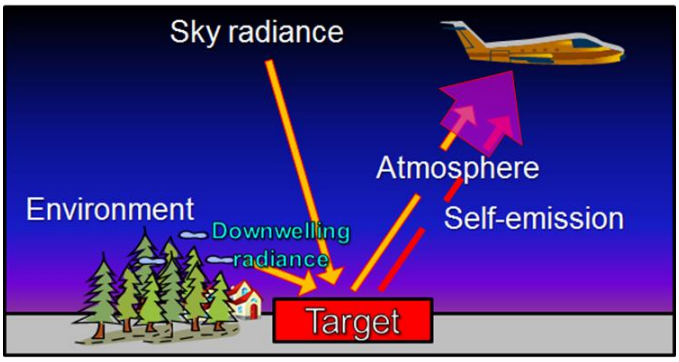

Figure 2 Schematic view of the various phenomena associated with thermal infrared in in airborne surveys of solid targets.

The spectral features associated with sky radiance, which are likely to be predominant within the reflection component, and atmospheric absorption/emission mostly results from infrared signals associated with gases. The spectral features that can be observed in a TIR spectrum of the sky and the atmosphere mostly correspond to ozone (O_3), water (H_2O) vapor, carbon dioxide (CO_2), methane (CH_4) and nitrous oxide (N_2O). It is well-known that the TIR spectral features associated with gases are pretty sharp and narrow compared with the infrared signature of solid materials such as minerals. To unveil the spectral features associated with minerals from TIR measurements, the respective contributions of self-emission and reflection in the measurement must be «unmixed». This procedure refers to temperature-emissivity separation (TES) [1]. Therefore, in order to achieve efficient TES and atmospheric compensation, airborne hyperspectral data should preferably be collected at high spectral resolution in order to discriminate the sharp spectral features associated with gases from the broad infrared signal typically associated with minerals.

In order to illustrate the potential of airborne TIR hyperspectral imaging for mineral mapping, an airborne survey was carried out above an open-pit chrysotile mine (not in operation anymore) using the Telops Hyper-Cam airborne system, a passive thermal infrared hyperspectral sensor based on Fourier transform spectroscopy, which provides high spectral resolution data. TES was carried out on the hyperspectral data in order to retrieve a thermodynamic temperature map and spectral emissivity data. Spectral «unmixing» of the emissivity data was then carried out using the spectral signatures of selected minerals which were obtained from commercial spectral libraries. Chemical maps of serpentine minerals (lizardite, serpentinite) and silicates (quartz) were obtained. The results illustrate how high resolution airborne TIR hyperspectral imaging can be successfully used to perform airborne mineral mapping of silicate minerals.

Experimental Information

The Telops Hyper-Cam Airborne Platform

All measurements were carried out using the Telops Hyper-Cam airborne platform. The Hyper-Cam-LW (longwave) is a lightweight and compact hyperspectral imaging instrument which uses Fourier Transfer Infrared (FTIR) technology. The Telops Hyper-Cam features a focal plane array (FPA) detector which contains 320×256 pixels over a basic 6.4°×5.1° field of view (FOV). For the

experiment, the FOV was extended to 25.6°×20.4° using a de-magnifying 0.25× telescope. In its airborne configuration, the spectral resolution is user-selectable up to 1 cm^{-1} over the 7.7 µm (1300 cm^{-1}) to 11.7 µm (855 cm^{-1}) spectral ranges. The Telops Hyper-Cam airborne platform is equipped with a global positioning system (GPS) and inertial motion unit (IMU) for geo-referencing and tracking of the aircraft movements in flight. An image-motion compensation (IMC) mirror uses the GPS/IMU data to compensate efficiently for the aircraft movements during data acquisition since acquiring a full datacube typically lasts about one second. The data includes all the relevant information for orthorectification and stitching. Visible images are simultaneously recorded along with the infrared datacubes using a boresight CCD camera on the airborne platform.

Figure 3 The Telops Hyper-Cam airborne platform.

Flight Conditions

The flight was carried out above an open-pit mine in Thetford Mines (Canada) in May 2013 around 5 PM at an altitude of 3000 feet and a speed of 110 knots. A visible image showing different regions of the surveyed area (GPS position: 46.077304, -71.312765) is shown in Figure 4. The mean ground elevation was in the order of 300 meters. Therefore, the average above ground level (AGL) was 800 meters leading to a ground pixel size of 1.25 m^2/pixel. A spectral resolution of 6 cm^{-1} was used which gives a total of 82 spectral bands equally spaced over the whole range covered by the FPA detector. A total of 6 parallel flight lines were required in order to survey the whole area. Ambient temperature and relative humidity at ground level were 11 °C and 26 % respectively.

Figure 4 Airborne overview of the Thetford Mines area.

Data Processing

Radiometric temperature maps were obtained by computing the mean values of each pixel put on a brightness temperature scale. Temperature emissivity separation (TES) was carried out by solving Eq.1 where L is the radiance measured at the sensor level, $\varepsilon_{\bar{\nu}}$ the target spectral emissivity, Dw the effective downwelling radiance on the target, L_{target} the target's self-emission which is function of its thermodynamic temperature as described by the Planck equation, τ_{atm} is the atmospheric transmittance, and L_{atm} the radiance associated with TIR self-emission of all atmospheric components.

Equation 1

$$L = \left[L_{target}\varepsilon_{\bar{\nu}} + Dw(1-\varepsilon_{\bar{\nu}})\right]\tau_{atm} + L_{atm}(1-\tau_{atm})$$

A smoothing criterion, similar to the one described in the work of Borel [2] was used to minimize both atmospheric and downwelling radiance contributions. Radiometric temperature maps were obtained by calculating, for each pixel, the mean brightness temperature value over whole detector spectral range.

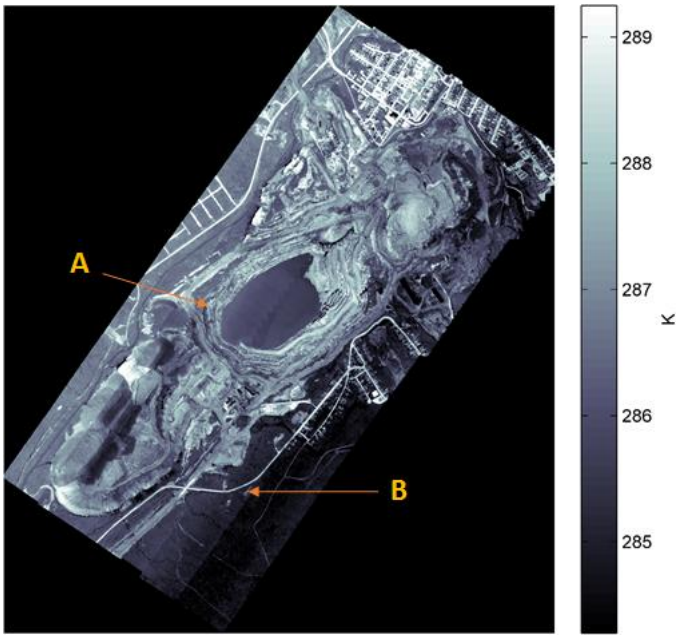

Figure 5 Radiometric temperature map of the Thetford Mines mining area. Two regions having different mineral compositions are labeled and will be discuss later.

Results and Discussion

Thermal Infrared Remote Sensing of Minerals

Common TIR broadband imaging systems provide a single temperature value which is function of the overall contribution of all investigated targets in the infrared detectors response range (e.g. 8-12 µm). However, as illustrated in Figure 2, the temperature measured by thermal infrared remote sensing is function of many parameters. Since no information about the different contributions (reflection, self-emission and atmospheric absorption) is available from a single value, the temperature results are in fact apparent temperatures. The radiometric temperature maps of the survey area, equivalent to what would be measured using a broadband TIR imaging airborne system, is shown in Figure 5. Relatively large thermal contrast (up to 6 K) can be seen throughout the whole area even over distances on the order of a few hundred meters. Such great temperature variations are unexpected for neighboring areas experiencing similar illumination conditions and are likely caused be emissivity differences, due to variations of the ground composition, rather than by temperature differences.

For most solid targets including minerals, emissivity has a spectral dependency. As an example of that, the reference spectral emissivity curve of quartz (SiO_2) is shown in Figure 6A. Two distinct spectral features can be observed at 1100 and 1200 cm^{-1} where the emissivity is the lowest. These broad features are associated with the Si-O asymmetrical stretching vibration of quartz [3]. The large absorption coefficient shifts associated with these molecular vibrations translates into a large refractive index (RI) shift. As a consequence of this steep RI shift, reflectivity is higher within these energy gaps that also often refer to Reststrahlen features. Within the high emissivity spectral ranges, the mineral behaves like a blackbody source (absorbing all incident radiation). Therefore, its self-emission dominates in these spectral ranges and the apparent temperature, i.e. brightness temperature, is closer to its thermodynamic temperature. From an airborne perspective, a target lying on the ground is facing the sky thus reflecting sky irradiance in low-emissivity spectral ranges. In high-emissivity spectral ranges, the atmospheric absorption from the air layer between the ground and the airborne sensor is the main contributor. Simulations for typical sky radiance, shown on a brightness temperature scale, and atmospheric transmittance are shown in Figure 6B. A simulation showing the resulting quartz spectrum seen from an airborne TIR HSI sensor is shown in Figure 6C. The latter figure also illustrates the relative width of the spectral features of gases and minerals highlighting the benefits of high spectral resolution for airborne thermal infrared hyperspectral mineral mapping.

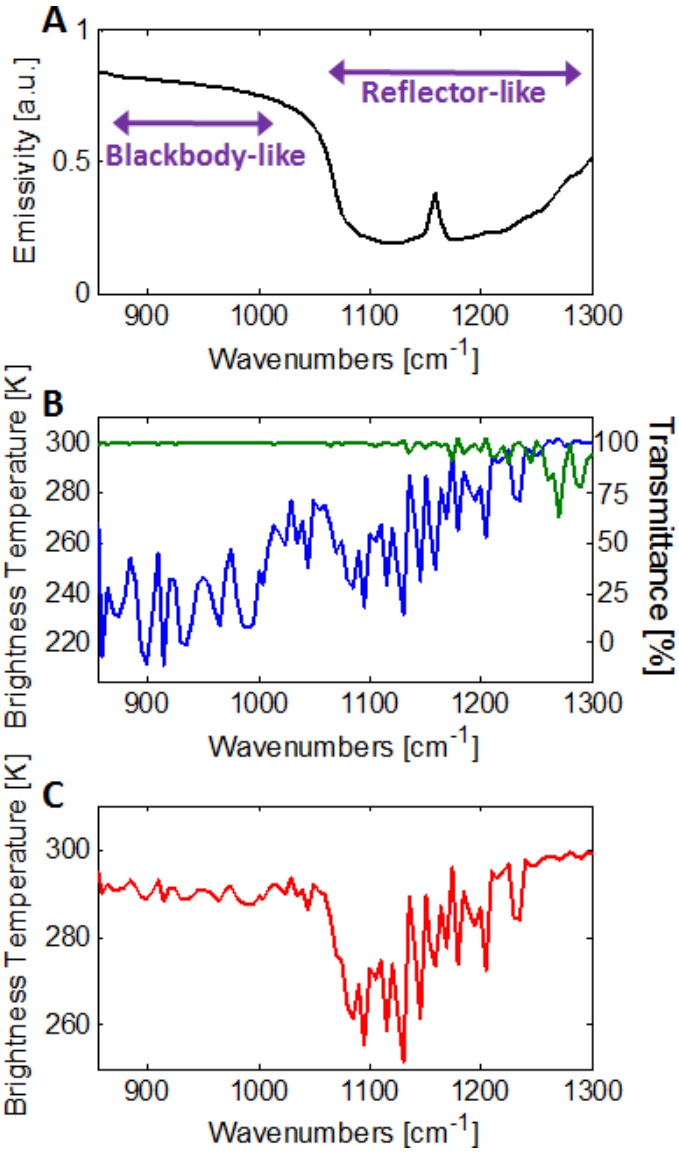

Figure 6 Reference spectral emissivity spectrum of quartz (A), spectral emissivity spectra of a typical sky (blue curve) and the atmospheric (green curve) at an AGL of 1000 m (B) and simulated quartz at 300 K seen from an airborne TIR HSI sensor (C).

Temperature-Emissivity Separation (TES)

In order to retrieve spectral emissivity information and gather knowledge about the mineral composition of the ground, Eq.1 must be solved efficiently. The infrared spectra of two (2) different locations, which are expected to have different geological contents, are shown in Figure 7. Their geographical positions, relative to the whole survey area, are labeled in Figure 5. The spectrum presented in Figure 7A corresponds to pixels located in the mining area. The broad spectral feature observed around 900-1075 cm^{-1} is likely associated with serpentine minerals that are expected to be present in great proportion within this area. The spectrum presented in Figure 7B corresponds to pixels located on a nearby road. Two broad spectral features around 1050-1275 cm^{-1} are likely associated with quartz minerals as shown previously. In both cases, sky radiance features can more or less be observed depending on the spectral emissivity properties of the ground material. The series of sharp peaks in the 1275-1300 cm^{-1} spectral range, common to both spectra, is associated with atmospheric absorption (mostly water vapor). In both cases, good agreement between the best fit of Eq.1 (green curve) and the measurements (blue curve) was obtained. The same procedure was applied to all pixels in order to retrieve the two outputs from a TES algorithm: a thermodynamic temperature map and a spectral emissivity datacube.

The thermodynamic temperature map obtained upon TES is shown in Figure 8. As expected, most temperature values are higher than their corresponding brightness temperature values since the reflection of a cold irradiance source, i.e. the sky, and the atmospheric contribution have been accounted for. The atmospheric absorption creates some kind of a systematic temperature offset in the radiometric temperature values. Since the TES procedure accounts for such effect, it is expected that thermodynamic temperature values are higher than their corresponding radiometric temperature values. As expected, vegetation and water areas are cooler then the roads, the city areas and bare rock surfaces found in the mining and tailing pounds areas. It can also be seen that the preliminary «thermal» contrasts seen on Figure 5, which were in fact emissivity contrasts, are also mitigated.

The spectral emissivity datacubes associated with the whole survey area contain the information about the mineral composition of the ground surface. However, as no pure substances are commonly encountered in the environment, spectral unmixing must be carried out on

the data in order to obtain chemical maps for individual minerals.

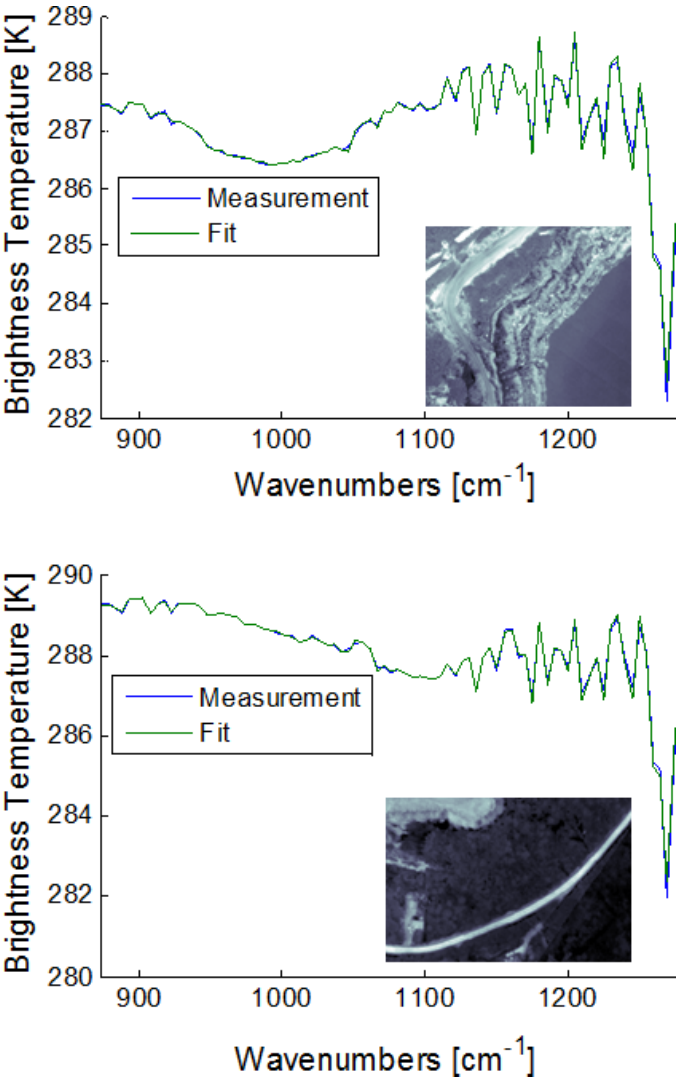

Figure 7 The infrared spectra of two selected locations, in the mining area (top, Region A) and a nearby road (bottom, Region B), is presented on a brightness temperature scale with their corresponding best fit of Equation 1.

Spectral Unmixing and Mineral Mapping

In order to achieve mineral mapping, the spectral emissivity datacube must be unmixed, i.e. one must estimate the relative contributions (coefficients $A, B \ldots$) of the different components ($\varepsilon_{\bar{\nu}_n}$), associated with the different minerals, within the overall emissivity signal ($\varepsilon_{\bar{\nu}_{tot}}$). Various strategies based on statistical, end-members, continuous wavelet analysis [4], or algebraic approaches can be used for the analysis of the emissivity data. In this case, a linear mixing approach was selected as expressed in Eq.2.

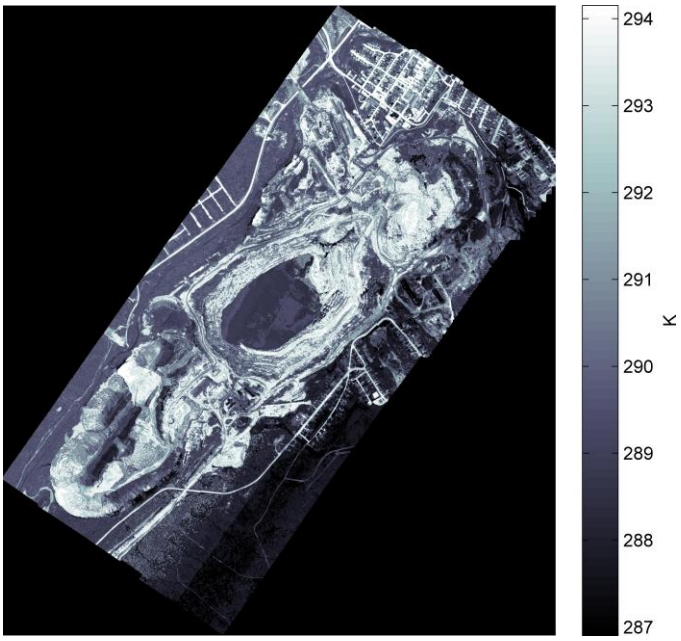

Figure 8 Thermodynamic temperature map as obtained after temperature-emissivity separation.

Equation 2

$$\varepsilon_{\bar{\nu}_{tot}} = A\varepsilon_{\bar{\nu}_1} + B\varepsilon_{\bar{\nu}_2} + C\varepsilon_{\bar{\nu}_3} + \mathrm{D}\varepsilon_{\bar{\nu}_n}$$

Linear unmixing of the spectral emissivity data was carried out using reference spectra from commercial libraries such as John Hopkins University (JHU), Jet Propulsion Laboratory (JPL) and United State Geological Survey (USGS). The component list comprised quartz (sand), calcite, lizardite, serpentinite (mostly antigorite) and magnesite ($MgCO_3$), granite, feldspar and dunite (mostly olivines). The spectral signature selection was carried out according to local geological information as well as recent work in a nearby area [4]. The reference spectra of a few minerals are shown in Figure 9 as well as the spectral emissivity data of the two selected locations retrieved by the TES procedure described earlier.

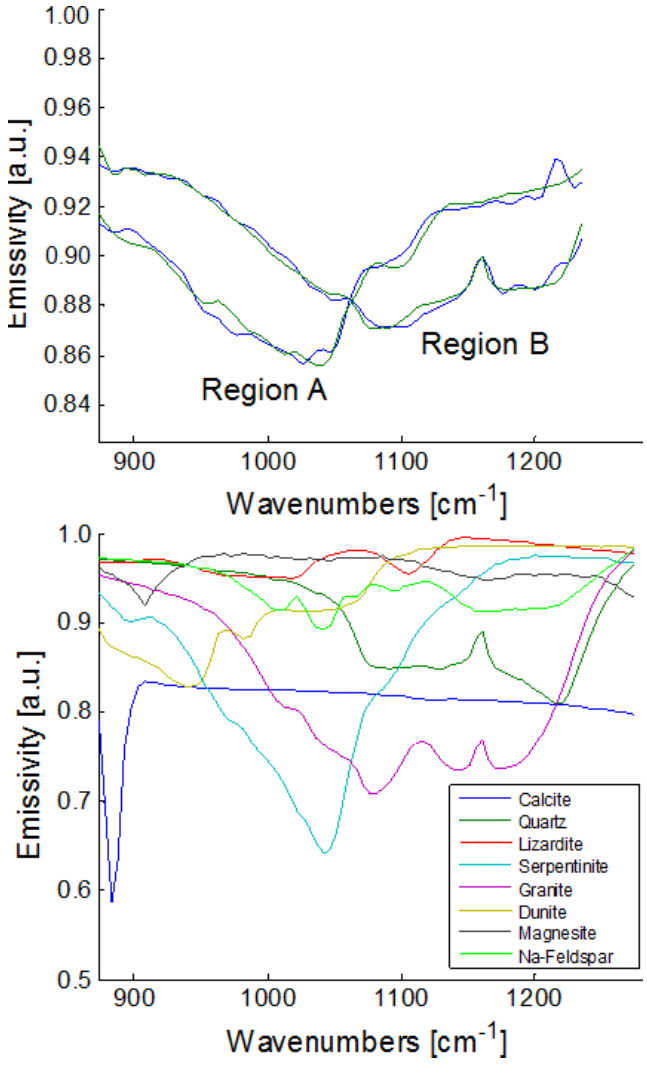

Figure 9 Spectral emissivity unmixing (top) of the signals associated with mining (Region A) and the road (Region B) areas. The blue curves correspond to the spectral emissivity curves obtained upon TES and the green curve correspond to the best fit of Eq.2. Reference spectra are shown (bottom) for comparison purposes.

Reasonably good matches were obtained between the estimated spectral emissivity data (blue curve) and the best fit from Equation 2 (green curve) as seen in Figure 9. Many factors can explain the disparities between the measurements and the fits such as the uncertainties in emissivity data retrieved from the TES algorithm or a mismatch between the encountered mineral polymorph and the one selected from the reference library. Nevertheless, the relative abundancies (coefficients in Eq.2) distribution could be successfully carried out for the selected minerals and typical results are shown in Figure 10 and Figure 11.

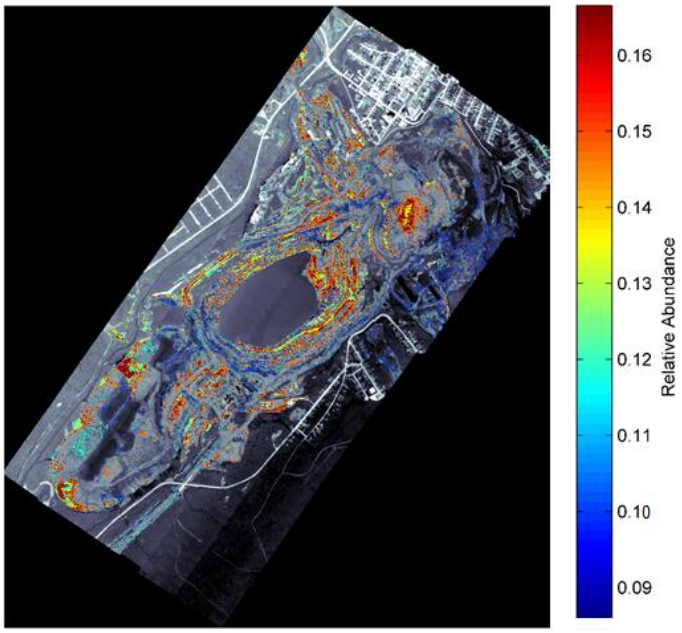

Figure 10 Serpentinite relative abundance map obtained from linear unmixing of the emissivity data. The results are displayed over the radiometric temperature map (grey scale) for clarity purposes.

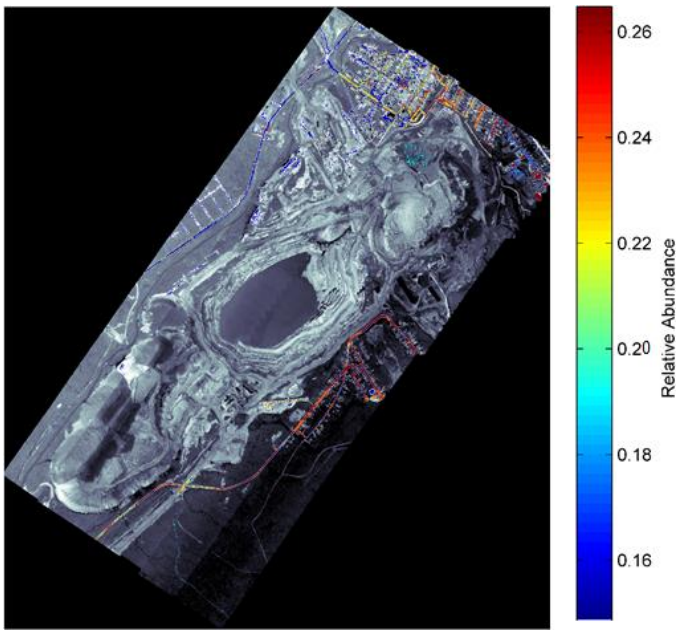

Figure 11 Quartz relative abundance map obtained from linear unmixing of the emissivity data. The results are displayed over the radiometric temperature map (grey scale) for clarity purposes.

Despite the uncertainties associated with the spectral unmixing approach used in this work, reasonable relative abundancies maps were obtained. A thematic mineral map, derived from the main (highest relative abundancies coefficient) component obtained for each

pixel is presented in Figure 12. As expected, serpentinite and lizardite are highly located in the mining area and in the tailing pounds where the mining residues are stored. As expected, both minerals are also co-registered spatially since the chrysotile milling process does not include separation of these two components. Dunite corresponds to bedrock, i.e. unaltered areas (incomplete or no serpentinization). Quartz spectral signature was exclusively detected outside of the mining area. Olivine and serpentine minerals are unlikely to be found associated with quartz minerals because of their different crystallisation processes. Quartz is often encountered in soils, sand and used in the production of many materials such as concrete and asphalt. Therefore, it is not surprising to obtain positive detection for quartz mineral in urban areas and roads [5]. The blank areas correspond to unstructured emissivity or undetermined components. The water pond seen in the center portion of the mining area and the vegetation mostly behave like a grey body, i.e. have no spectral features and an emissivity lower than unity, making their detection based on spectral features very difficult in the TIR spectral range.

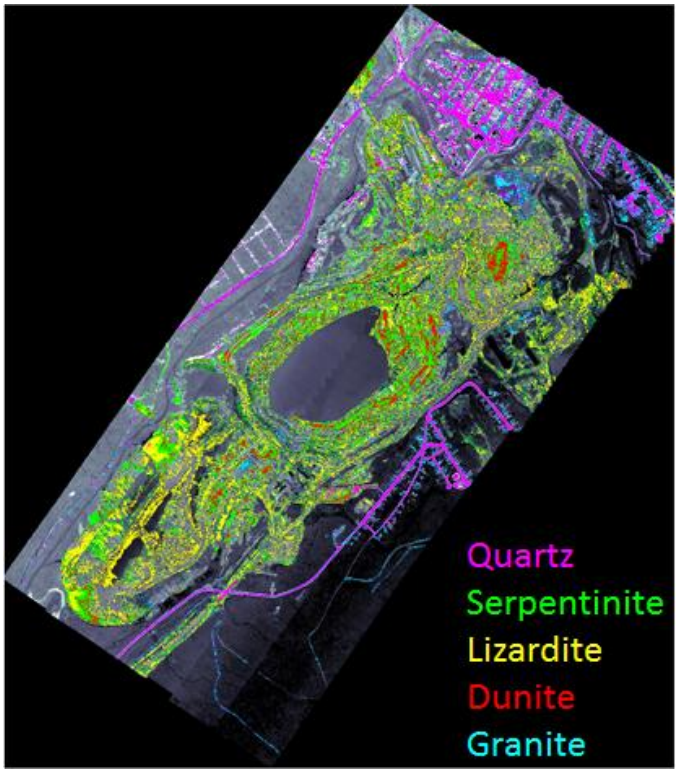

Figure 12 Thematic mineral map of the Theford Mines area.

Conclusion

Airborne TIR hyperspectral data recorded, at a high spectral resolution allows efficient compensation of atmospheric and sky reflection contributions in the measured signal. The spectral emissivity could be successfully unmixed using basic geological components expected to be found in the area. The chemical maps derived from the emissivity data are in good agreement with the expected results illustrating the benefits of airborne thermal infrared HSI for mineral mapping of silicate minerals.

References

[1] A.R. Gillespie, *et al.*, Temperature/Emissivity Separation Algorithm Theoretical Basis Document, Version 2.4, NASA, 64 p (1999).

[2] C.C. Borel, ARTEMISS – an Algorithm to Retrieve Temperature and Emissivity from Hyper-Spectral Thermal Image Data, *28th Annual GOMACTech Conference.*, Hyperspectral Imaging Session, (2003).

[3] B.J. Saikia, *et al.*, Fourier transform infrared spectroscopic estimation of crystallinity in SiO_2 based rocks, *Bull.Mater.Sci.*, **31**, 775 (2008).

[4] B. Rivard, *et al.*, First geological case study of the airborne longwave hyperspectral Hyper-Cam system, Thetford Mines, Quebec, *IGARSS Conference*, 4025 (2014).

[5] M.A. Gagnon, *et al.*, Airborne Thermal Hyperspectral Imaging of Urban and Rural Areas, *IGARSS Conference*, 1369 (2014).

Telops Inc.
100-2600 St-Jean Baptiste ave.
Québec (QC), Canada
G2E 6J5

Tel.: +1-418-864-7808
Fax. : +1-418-864-7843
sales@telops.com
www.telops.com